Catalysis Today 172 (2011) 136–142

Contents lists available at ScienceDirect

Catalysis Today

journal homepage: www.elsevier.com/locate/cattod

RhNi nanocatalysts for the CO_2 and $CO_2 + H_2O$ reforming of methane

M. García-Diéguez, I.S. Pieta, M.C. Herrera, M.A. Larrubia, L.J. Alemany*

Departamento de Ingeniería Química, Facultad de Ciencias, Campus de Teatinos, Universidad de Málaga, Málaga E-29071, Spain

ARTICLE INFO

Article history:
Received 30 November 2010
Received in revised form 31 January 2011
Accepted 4 February 2011
Available online 26 March 2011

Keywords:
Dry reforming
Steam reforming
Methane
Rhodium

ABSTRACT

Monometallic and bimetallic RhNi nanocatalysts, supported on a nanofibrous alumina, employed for H_2(+CO) production by CO_2 and $CO_2 + H_2O$ reforming of methane were prepared and tested under reaction conditions. The catalysts were characterized before and after reaction by conventional methods. The influence of the incorporation of Rh to Ni/Al_2O_3 catalysts and presence of H_2O in the reaction were analyzed. Characterization results showed that the incorporation of Rh in the formulation promotes the reducibility and stability of Ni particles, avoids Ni aggregation and inhibits the net carbon formation. RhNi supported nanocatalysts are highly active and stable systems for the CO_2 and $CO_2 + H_2O$ reforming of methane. Low Rh loading, in an atomic ratio 1:100 (Rh:Ni), in Ni-based catalysts allowed an improvement in the reaction stability as well as in the selectivity towards H_2 and CO instead towards coke. The incorporation of water in the feed stream produces a drastic decrease in the global carbon formation and the quantity incorporated can be tuned to obtain different H_2/CO ratios.

© 2011 Elsevier B.V. All rights reserved.

1. Introduction

The production of hydrogen and *syngas* can be carried out by steam reforming, partial oxidation, dry reforming or by a mixture of them as the autothermal reforming or the mixed CO_2 and H_2O reforming [1,2]. Steam reforming is typically the preferred process for hydrogen production in industry; however, it has one of the highest emissions among the reforming processes [1].

Water can be replaced by CO_2, to produce *syngas* with lower H_2/CO ratio values, which are appropriate for the synthesis of valuable oxygenated chemicals [3–10]. Due to the high endothermic nature of this reaction it can be used in energy transfer from solar energy to chemical energy, energy storage in the form of CO and H_2, and transporting nuclear energy [10]. When a source of CO_2 is available it is likely that CO_2 reforming will become a promising industrial process, reusing greenhouse effect gases as CO_2 and CH_4. The principal drawback of this reaction is the high carbon formation, principally on Ni-based catalysts the most common used catalysts for reforming reactions [5,11,12], leading to the catalyst deactivation. Dry reforming requires the use of stable and effective catalysts, resistant to coking; hence investigations should be focused on the metal activity, the resistance to coke formation and the type of support that improves the catalyst efficiency [5,13]. In previous works [14–16] we have reported the use of bimetallic PtNi catalysts supported on a synthetic nanofibrous alumina for the dry reforming of methane (DRM) which are stable and highly active for this reaction. It was found that the addition of Pt to Ni catalysts and the use of the nanofibrous alumina as support lead to the formation of bimetallic PtNi particles enriched on the surface by Pt [16], which promote the dispersion, inhibit the net carbon formation and improve the stability during the DRM reaction.

When the CO_2 is available and the pressure in the system is not high enough to obtain adequate H_2/CO ratio values for the methanol synthesis, the $CO_2 + H_2O$ reforming seems to be an interesting process for the production of *syngas* with the appropriate characteristics [17]. Moreover, this reaction may be feasible with natural gas containing CO_2 or with exhaust gases from other processes.

The aim of the present contribution is the development of highly stable and active RhNi catalysts supported on nanofibrous alumina for H_2(+CO) production during the DRM and $CO_2 + H_2O$ reforming of methane (DRM + H_2O).

2. Experimental

2.1. Catalysts preparation

A synthesized nanofibrous γ-Al_2O_3 was employed as support (A_{BET} = 300 $m^2\,g^{-1}$ and V_P = 1 $cm^3\,g^{-1}$). The nanostructured alumina was prepared using $NaAlO_2$ as precursor and employing a non-ionic surfactant to control the size and morphology of the support. The synthesis procedure, as well as the characterization data for this alumina has been already reported elsewhere [14,15]. Before the catalysts preparation, the support was finally treated in air at 1073 K for 2 h (0.17 K s^{-1}).

* Corresponding author. Tel.: +34 952 13 1919; fax: +34 952 13 1919.
E-mail address: luijo@uma.es (L.J. Alemany).

0920-5861/$ – see front matter © 2011 Elsevier B.V. All rights reserved.
doi:10.1016/j.cattod.2011.02.012

Monometallic and bimetallic RhNi catalysts were prepared by simultaneous incipient wetness impregnation of the support employing as precursors of Ni and Rh $Ni(NO_3)_2{\cdot}6H_2O$ and $Rh(H_2O)(OH)_{3-y}(NO_3)_y$ ($y = 2$–3), respectively. Monometallic Ni (4 at nm^{-2}; labeled as $4Ni/Al_2O_3$) and Rh (0.4 at nm^{-2}; labeled as $0.4Rh/Al_2O_3$) catalysts were prepared, as well as a bimetallic noble metal–Ni catalyst with 4 at nm^{-2} of Ni and 0.04 at nm^{-2} of Rh ($0.04Rh4Ni/Al_2O_3$). After the impregnation the catalysts were treated in stagnant air at 373 K overnight and then at 1023 K for 5 h (0.17 K s^{-1}).

2.2. Characterization

X-ray powder diffraction data have been recorded with an X'Pert MPD PRO diffractometer (PANalytical) using CuKα1 radiation (λ = 1.54059 Å) and a Ge(1 1 1) primary monochromator. The X-ray tube worked at 45 kV and 35 mA. The measurements were done from 10° to 70° (2θ). TEM images were taken with a Philips CM 200 of 200 kV; the samples were prepared using ethanol as dispersant. X-ray photoelectron spectra were recorded on a Physical Electronic 5701 equipped with a PHI 10-360 analyzer using the MgKα X-ray source. Binding energy (BE) values were referred to the C1s peak (284.8 eV) from the adventitious carbon for the catalysts before reaction and to the Al2p peak for the catalysts after reaction. All deconvolutions of experimental curves were done with Gaussian and Lorenzian line fitting, minimizing the (χ^2) chi-square values. The carbon content of the catalysts after reaction was obtained via elemental analysis technique using an Elemental Analyzer Perkin-Elmer 2400 CHN. The characterization of the carbon formed was performed after the reactivity tests of the DRM or DRM + H_2O reactions realized at the same temperature and time on stream. Temperature-programmed reduction (TPR) of the fresh catalysts was performed on a Micromeritics Autochem II 2920 with a thermal conductivity detector (TCD). Samples were reduced in a flow of H_2 diluted in Ar (10%) at 50 N cm^3 min^{-1} and heated from room temperature to 1323 K (10 K min^{-1}).

2.3. Reactivity

Steady state experiments were carried out in a Microactivity-Reference reaction system from PID Eng&Tech (Spain) at atmospheric pressure in a temperature range between 673 and 1023 K. A tubular fixed bed stainless steel reactor (i.d. 9 mm) with 100 mg of catalyst (250–420 μm) was employed. The total gas flow rate was kept constant at 0.83 N cm^3 s^{-1} with stoichiometric composition diluted in He ($CH_4/CO_2/He = 20/20/60$ for the DRM and $CH_4/CO_2/H_2O/He = 3/1/2/9$ for the DRM + H_2O). The space velocity and the contact time were 6000 h^{-1} and 0.8 g h mol^{-1}, respectively; operating under plug flow conditions. Preliminary reactivity tests with different catalyst particle sizes and dilutions were performed to confirm the non-existence of heat or mass transfer limitations.

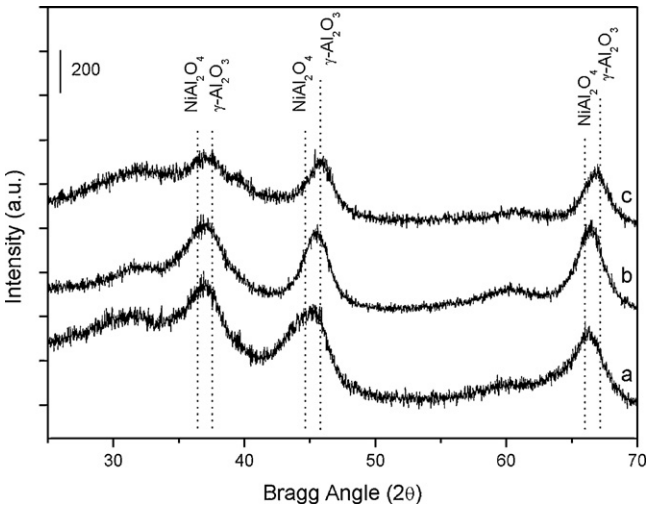

Fig. 1. XRD patterns of the catalysts before reaction. (a) $4Ni/Al_2O_3$; (b) $0.04Rh4Ni/Al_2O_3$; (c) $0.4Rh/Al_2O_3$.

Before reaction, catalysts were activated in situ with H_2 (3% in He, 0.5 N cm^3 s^{-1}) at 973 K for 2 h. The reaction temperature was measured with a thermocouple placed in the reactor bed. The reactor effluent was analyzed by GC (Agilent 4890D) equipped with TCD and FID detectors. Stability runs under DRM reaction conditions were performed at 973 K. C, H and O balances were closed with deviations lower than 5%.

3. Results and discussion

3.1. Characterization

The XRD patterns for the fresh catalysts are presented in Fig. 1. All the diffractograms present the characteristic broad lines related to pseudo-amorphous gamma Al_2O_3 (JCPDS 75-0921), which were slightly shifted to lower Bragg angle for the Ni-containing catalysts, probably due to the presence of Ni aluminate (JCPDS 01-1299). No signal associated with Rh was observed suggesting that Rh is well dispersed or the quantity of Rh is too low to be detected by XRD. Particles of Rh or Ni were not detected by TEM either, as can be observed in Fig. 2, where just the nanofibrous morphology of the support (fibers of 2–6 nm in diameter and 60 nm in length) can be distinguished. Fig. 3 shows the XRD patterns for the catalysts after the DRM reaction. Apart from the signals detected before reaction two new signals were registered for the Ni-catalysts, metallic Ni (JCPDS 70-1849) and graphitic carbon (JCPDS 89-8489). Average particle size of Ni^0 for the Ni-containing catalysts was calculated by the Scherrer equation, the results obtained are summarized in Table 1. It should be noticed that the Ni^0 cluster size is 52% lower

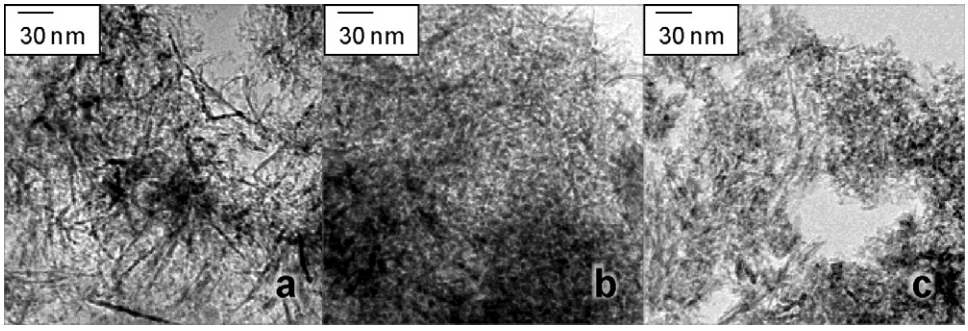

Fig. 2. TEM images of the catalysts before reaction. (A) $4Ni/Al_2O_3$; (B) $0.04Rh4Ni/Al_2O_3$; (C) $0.4Rh/Al_2O_3$.

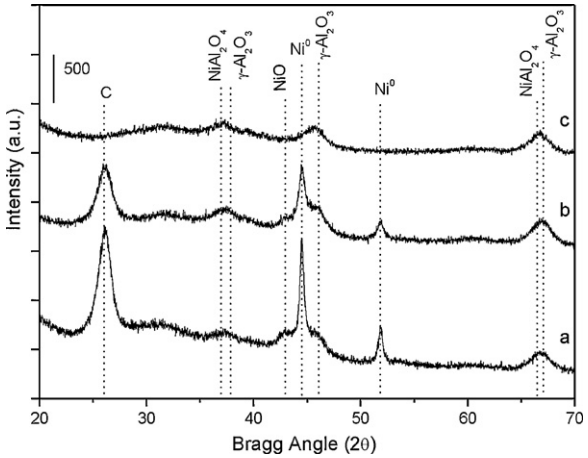

Fig. 3. XRD patterns of the catalysts after the DRM reaction. (a) $4Ni/Al_2O_3$; (b) $0.04Rh4Ni/Al_2O_3$; (c) $0.4Rh/Al_2O3$.

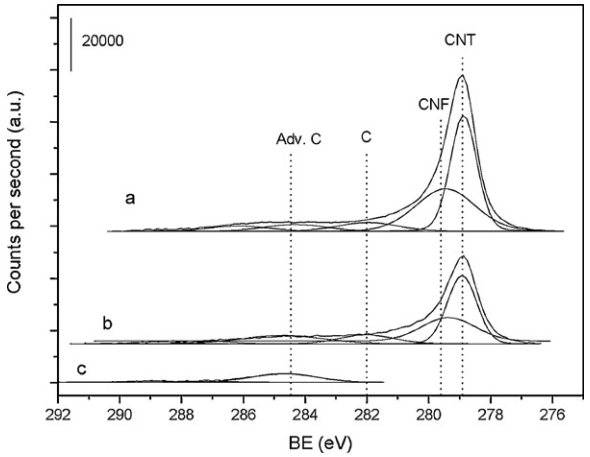

Fig. 5. C1s core level spectra of catalysts after the DRM reaction (XPS). CNT: carbon nanotubes; CNF: carbon nanofibers; C: filamentous carbon; Adv. C: adventitious carbon. (a) $4Ni/Al_2O_3$; (b) $0.04Rh4Ni/Al_2O_3$; (c) $0.4Rh/Al_2O_3$.

Table 1
Average particle size of Ni^0 and carbon content of the catalysts after reaction.

Catalyst	$D_P Ni^0$ (nm)[a]	C (wt%)[b]	
		DRM	DRM + H_2O
$4Ni/Al_2O_3$(N)	23	45	2
$0.04Rh4Ni/Al_2O_3$(N)	11	27	2
$0.4Rh/Al_2O_3$(N)	–	0.3	0.4

[a] Average particle size of Ni^0, calculated by the Scherrer equation.
[b] Carbon content of the catalysts after the DRM and DRM + H_2O reactions, obtained by elemental analysis.

when Rh is incorporated in comparison with the monometallic Ni catalyst. This latter result shows that the addition of a small amount of Rh and the morphology of the support affect the dispersion of Ni, as has been reported for PtNi catalysts supported on nanofibrous alumina [14,15].

The graphitic carbon observed by XRD for the Ni-catalyst comes from the parallel reactions to DRM as methane cracking and Boudouard reactions. It is important to point out that the intensity of the principal XRD signal related to carbon is lower for the bimetallic catalyst, in agreement with the carbon content obtained after the DRM reaction by elemental analysis (Table 1), which is 40% lower for the bimetallic RhNi catalyst with respect to the monometallic Ni catalyst. Moreover, the TEM images taken for the catalysts after reaction (Fig. 4) show an apparent reduction in the carbon formation for the catalysts containing Rh. The nature of the carbon observed is associated with carbon nanotubes (CNT) or nanofibers (CNF). For the monometallic Rh catalyst the amount of carbon detected by XRD, elemental analysis (0.3 wt%) or TEM was practically negligible.

In order to characterize the nature of the carbon formed during the DRM reaction the C1s core level spectra of the catalysts after reaction were registered (Fig. 5). All the spectra present two weak signals registered at 284.8 eV and 282.2 eV, the latter almost negligible for the $0.4Rh/Al_2O_3$ catalyst, which are associated with adventitious carbon from the analysis and filamentous carbon formed during reaction above the catalyst surface without physical contact, creating a differential charge effect [5]. In addition to these signals, for the Ni-containing catalysts, two more signals were registered at 278.8 eV and 280.0 eV. The first one, with the highest proportion, is assigned to the formation of CNT and the second one to the presence of CNF [14,15]. It is important to point out that the relative contribution and the intensity of the signals at 278.8 eV and 280.0 eV considerably decreased for the bimetallic RhNi catalyst. Furthermore, the spectra of the monometallic Rh catalyst did not present additional signals to those of adventitious and filamentous carbon, indicating that the net carbon formation for this catalyst during the DRM reaction is minimal, in agreement with the data presented above.

It is known that the rate of carbon formation is a process that depends on the structure of the metallic phase. It is inhibited in the presence of small and well disperse particles [18–20]. Additionally, the carbon formed can be partially removed by gasification with CO_2 in the presence of noble metals [21]. Characterization results indicate that when Rh is added to the Ni catalyst together with the promotion of the carbon gasification by CO_2, a synergic effect is created between Rh and Ni, through the interaction between metal centers, which is capable of increasing the dispersion and consequently diminishing the net rate of carbon formation.

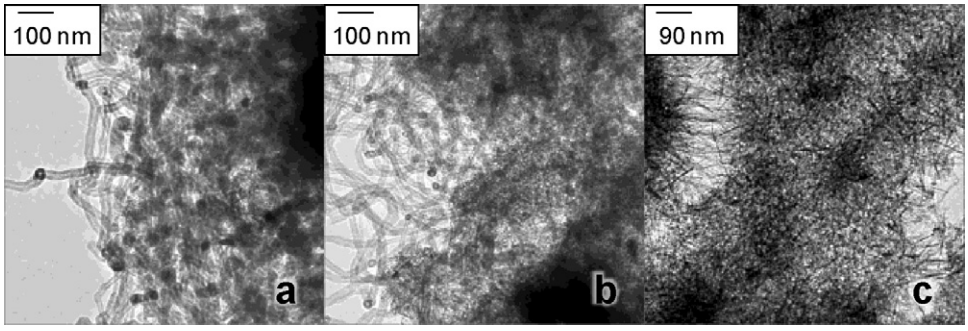

Fig. 4. TEM images of the catalysts after the DRM reaction. (A) $4Ni/Al_2O_3$; (B) $0.04Rh4Ni/Al_2O_3$; (C) $0.4Rh/Al_2O_3$.

Table 2
Binding energy (BE) and surface atomic ratios for the RhNi catalysts before (BR) and after (AR) reaction of the DRM, region Ni2p$_{3/2}$.

Catalyst	Ni 2p$_{3/2}$ [a]		
		BR	AR
4Ni/Al_2O_3(N)	Ni^0	–	852.9 (25)
	NiO	855.3 (32)	854.6 (25)
	$NiAl_2O_4$	856.1 (68)	856.1 (50)
	Ni/Al[b]	0.09	0.02
0.04Rh4Ni/Al_2O_3(N)	Ni^0	–	853.0 (46)
	NiO	855.5 (78)	855.8 (39)
	$NiAl_2O_4$	857.0 (22)	856.6 (15)
	Ni/Al[b]	0.07	0.03

[a] Binding energy (±0.2 eV), in brackets relative population of the species expressed in %.
[b] Surface atomic ratios.

Table 3
Binding energy (BE) and superficial atomic relations for the RhNi catalysts before (BR) and after (AR) reaction of the DRM, region Rh3d$_{5/2}$.

Catalyst	Rh 3d$_{5/2}$ [a]		
		BR	AR
0.04Rh4Ni/Al_2O_3(N)	Rh^0	–	307.3 (30)
	Rh_2O_3	309.3 (100)	308.9 (70)
	Rh/Al[b]	3×10^{-4}	9×10^{-4}
0.4Rh/Al_2O_3(N)	Rh^0	307.4 (10)	306.8 (100)
	Rh_2O_3	308.9 (90)	–
	Rh/Al[b]	0.01	0.01

[a] Binding energy (±0.2 eV), in brackets relative population of the species expressed in %.
[b] Surface atomic ratios.

The surface of the catalysts before and after the DRM reaction was characterized by XPS. The binding energy (BE) values and the surface atomic ratios (Ni/Al and Rh/Al) for the Ni2p$_{3/2}$ and Rh3d$_{5/2}$ core electrons are presented in Tables 2 and 3, respectively. For the Ni-containing catalysts two different Ni species were detected with BE at 855.3–855.5 eV and 856.1–857.0 eV, which are associated with Ni^{2+} as NiO and $NiAl_2O_4$, respectively [5,22]. The relative proportion of NiO for the bimetallic catalyst (78%) was higher than that for the monometallic Ni catalyst (32%), suggesting that the presence of Rh could inhibit the Ni spinel formation, which is hardly reduced [23] diminishing the number of active sites for the DRM reaction.

For the Ni-catalysts after the DRM reaction the species detected before reaction were also observed with a slight shift in BE, registering values of 854.6–855.8 eV and 856.1–856.6 eV for NiO and $NiAl_2O_4$, respectively. Additionally to these signals, a peak at a BE of 852.9–853.0 eV was detected, which is related to the presence of Ni^0 [5]. It is worth noticing that the proportion of metallic Ni in the bimetallic catalyst is higher than in the monometallic Ni catalyst, indicating that the addition of Rh promotes the reducibility of Ni. This effect has been observed also for PtNi catalysts supported on nanofibrous alumina [2,14–16], where the presence of Pt modifies the chemical behavior of Ni, increasing its reducibility. Improvements in Ni reducibility have also been reported for NiO–MgO solid solutions [24] catalysts promoted by Pt, which are addressed to a spillover effect of hydrogen from the second metal to Ni. Moreover, the Ni/Al surface atomic ratio obtained for the monometallic Ni catalyst after reaction is 78% lower than that registered before reaction, indicating that the number of Ni species on surface available for catalysis diminishes during the DRM reaction. For the bimetallic NiRh catalyst the Ni/Al surface atomic ratio decreases in 57% with respect to before reaction, less than for the monometallic Ni catalyst, suggesting an enrichment by Rh on the catalyst surface after reaction that stabilizes the Ni surface species, inhibiting the net carbon formation and avoiding the migration of the Ni into the alumina support.

In the Rh3d$_{5/2}$ core electrons region for the bimetallic RhNi catalyst before reaction, only one signal was detected at 309.3 eV, which is related to Rh^{3+} as Rh_2O_3 [25]. After reaction an additional species to Rh_2O_3 (308.9 eV – 70%), observed before reaction, was registered at 308.9 eV, which is associated with metallic Rh [26] whose relative contribution was 30%. For the monometallic Rh catalyst before reaction two different Rh species were detected Rh^0 and Rh_2O_3 with BE at 307.4 eV (30%) and 308.9 eV (70%), respectively. After reaction only one signal was observed at 306.8 eV, associated with metallic Rh. The Rh/Al surface atomic ratios registered for the Rh-containing catalysts do not change significantly before and after reaction, ensuring the availability of Rh species during the DRM reaction on the catalysts' surface.

In order to study the reducibility of Ni the temperature-programmed reduction (TPR) experiments were realized for the Ni-containing catalysts, the TPR profiles are shown in Fig. 6. The

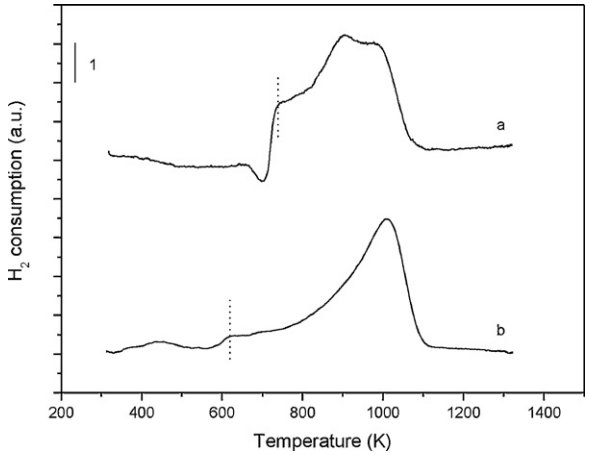

Fig. 6. TPR profiles of the fresh Ni-containing catalysts. (a) 4Ni/Al_2O_3; (b) 0.04Rh4Ni/Al_2O_3.

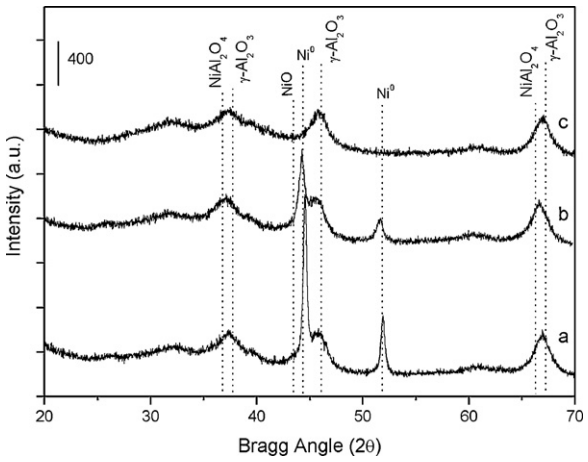

Fig. 7. XRD patterns of the catalysts after the DRM + H_2O reaction. (a) 4Ni/Al_2O_3; (b) 0.04Rh4Ni/Al_2O_3; (c) 0.4Rh/Al_2O_3.

TPR profile of the Ni monometallic catalyst shows three broad peaks located at 742, 912 and 996 K. The width of the first peak (742 K) suggests that it can be related to the reduction of non-crystalline NiO species, in agreement with the XRD data. The temperature of reduction for these species is higher than for bulk NiO (600–658 K [27,28]). This is due to the presence of aluminum ions of the support, which inhibit the propagation of nucleation; as has also been reported by Scheffer et al. [29]. The maximum peak located at 912 K is associated with the reduction of NiO located close to the surface and surrounded by a high number of aluminum ions [29]. The third peak, typical for Ni/Al_2O_3 catalysts calcined at high temperature, is related to the $NiAl_2O_4$ phase, which is formed through diffusion of Ni ions into the support [28–31].

The RhNi catalyst presents a TPR profile with a broad signal with a maximum peak at 1006 K and one shoulder at 617 K, together with two weak signals at 458 and 263 K. The peak at 1006 K corresponds to $NiAl_2O_4$ and the shoulder at 661 K can be related to the reduction of non-crystalline NiO species, shifted to lower temperature due to an interaction between Rh and Ni, in agreement with the XPS results. The other weak signals can be associated with three-dimensional RhO_X and two-dimensional surface RhO_X phase [32], respectively. It is worth noticing that the asymmetry of the signals suggests that the reduction of another kind of Ni species, as NiO surrounded by aluminum from the support, cannot be excluded.

It has been reported that another way to reduce the net carbon formation is the addition of water to the DRM reaction: the mixed CO_2 and steam reforming [4,7,33–35]. In order to study the effects of the incorporation of water the RhNi series of catalysts described above were also tested for the DRM + H_2O and subsequently characterized by XRD and Elemental Analysis. The XRD patterns for the catalysts after the DRM + H_2O reaction are shown in Fig. 7. All of the diffractograms present the lines registered after the DRM reaction with the exception of those related to carbon, indicating the formation of graphitic carbon has been hindered by the presence of water. This latter result is in concordance with the contents of carbon registered by elemental analysis (Table 1), which have diminished more than a 90% with respect to those registered after the DRM reaction (without water). Choudhary and Rajput [34] reported that in the mixed CO_2 and H_2O reforming on NiO–CaO catalysts the formation of carbon is drastically inhibited. It is also worth noticing that the average cluster size of Ni^0 after the DRM + H_2O reaction is not modified, keeping the same dispersion after reaction for the DRM and DRM + H_2O. Apparently, for the mixed reforming not only the particle size affects the global carbon formation, the presence of water allows the gasification of the carbon formed, being more effective than the gasification by only CO_2.

3.2. Reactivity

Fig. 8 shows the activity and stability results registered for the RhNi catalysts during the DRM reaction ($CH_4/CO_2/He = 1/1/3$) at 573–973 K together with the equilibrium values, obtained by the minimization of the Gibbs free energy method taking into account CH_4, CO_2, H_2, CO, H_2O and He as species in the reaction system; solid carbon was not considered. CH_4 and CO_2 conversion values are lower than those from equilibrium and the CO_2 conversion is higher than CH_4 conversion for the whole temperature range (Fig. 8A and B), indicating the presence of side reactions as has been also observed for other Ni-based catalysts [2,14,15]. CH_4 conversion values tend to be higher for the monometallic Ni catalyst than for the Rh-containing catalysts at 773–873 K, as a consequence the H_2/CO ratios (Fig. 8C) registered are also higher, however, when the temperature is increased the selectivity to H_2 for this catalyst decreases as well as the CH_4 conversion with respect to the conversion registered for the other catalysts, probably due to the loss of Ni species on the surface (Table 2) and the sintering of Ni (D_PNi^0 after reaction, Table 1). It has been reported that the DRM of methane is a structure sensitive reaction where the rate of methane activation increases along with the dispersion [36]. For the Rh-containing catalysts the selectivity, expressed as the H_2 to CO ratio, slightly decreases at high temperature and at a lower rate than for the Ni monometallic catalyst, which can be due to the higher availability of active species on the surface for this catalysts (in agreement with XPS data, Tables 2 and 3).

The stability of the RhNi catalysts for the DRM reaction at 973 K was also studied, the results obtained for the conversion of CO_2 as a function of the time on stream for the first 14 h are presented in Fig. 8D. It can be observed that even when small quantities of Rh (0.04 at nm^{-2}, Rh:Ni atomic ratio of 1:100 equivalent to 0.2 wt%) were added the stability of this system for the DRM is considerably improved with respect to the monometallic Ni catalyst. The loss of CO_2 conversion per hour on stream is decreased from 1.3% h^{-1} for the monometallic Ni catalyst to 0.6% h^{-1} for the bimetallic RhNi catalyst. It is also important to point out that the monometallic Rh catalyst is quite stable for the DRM reaction, registering a loss of CO_2 conversion per hour of 0.2% h^{-1}.

Apparently the carbon formed and carbon nature, with the bimetallic RhNi catalysts does not inhibit the activity for the DRM reaction, probably the carbon does not diffuse in the same extent than for the monometallic Ni catalyst because of the presence of smaller Ni^0 particles in the bimetallic catalysts. Normally the carbon diffusion is more easily performed in bigger Ni particles [20] and is not present on noble metal particles [2]. As the carbon does not diffuse through Rh, the Rh active centers are not covered during reaction ensuring the presence of active sites and consequently the temporal stability of the catalysts during the DRM reaction. Moreover, the presence of Rh modifies the superficial electronic density of the Ni based catalyst, by the Ni–Rh interaction, facilitating the activation of the reactants and the removal of the carbon formed.

The RhNi catalysts were also tested in DRM + H_2O reaction ($CH_4/CO_2/H_2O/He = 3/1/2/9$) at 973 K and 1023 K. The CH_4 and CO_2 conversion values, as well as the H_2/CO ratios are shown in Table 4. The CO_2 conversion values are lower than those of CH_4 conversion at both temperatures, indicating that at these conditions the activation of H_2O (steam reforming) seems apparently more favored than the activation of CO_2 (dry reforming) and probably a CO_2 recycle would be necessary in this process to make use of all the CO_2 available. It is also important to point out that the reactivity levels reached with the Rh-containing catalysts for the DRM + H_2O reaction were higher than those for Ni monometallic catalyst. Apparently, the Rh allows a higher activation of the H_2O and CH_4, giving higher methane conversions and H_2/CO ratios.

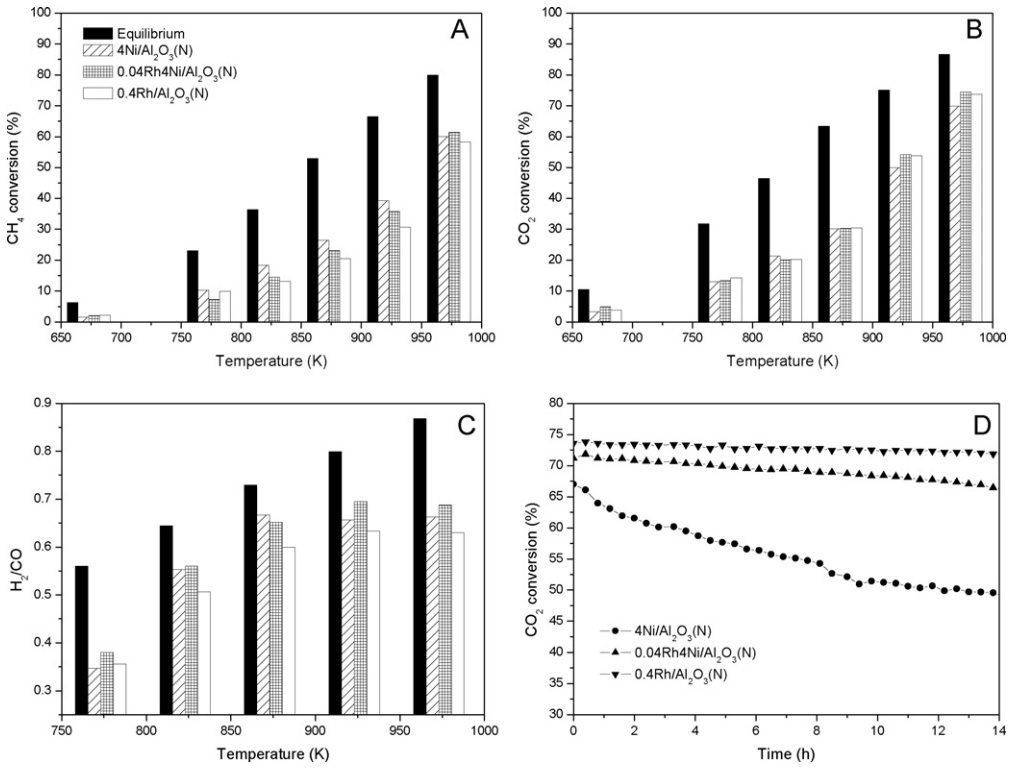

Fig. 8. Activity and stability results during DRM reactions ($CO_2/CH_4/He = 1/1/3$, GHSV = 6000 h^{-1}, W/F = 0.8 g h mol^{-1}, atmospheric pressure). (A) CH_4 conversion vs. temperature; (B) CO_2 conversion vs. temperature; (C) H_2/CO ratio vs. temperature; (D) CO_2 conversion vs. time on stream (973 K).

Table 4
Conversion and selectivity values registered for the RhNi catalysts during the DRM + H_2O reaction.

Catalizador	X_{CH_4} [a]		X_{CO_2} [a]		H_2/CO	
	973 K	1023 K	973 K	1023 K	973 K	1023 K
$4Ni/Al_2O_3(N)$	82	89	23	42	1.46	1.49
$0.04Rh4Ni/Al_2O_3(N)$	84	89	22	44	1.67	1.63
$0.4Rh/Al_2O_3(N)$	91	93	11	39	1.81	1.78

[a] CH_4 and CO_2 conversions ($CH_4/CO_2/H_2O/He = 3/1/2/9$), GHSV = 6000 h^{-1} and W/F = 0.8 g h mol^{-1}.

In addition, it is interesting to note that the H_2/CO ratios obtained with the DRM + H_2O reaction on these catalysts are considerably higher (300%) than those registered for the DRM reaction at 973 K, thanks to the extra source of hydrogen, the H_2O. Besides, the high selectivity towards H_2, probably due to the significant contribution of the WGSR, instead of towards carbon makes of this process a valuable alternative to attain *syngas* with the appropriate characteristics for different processes that require high H_2/CO ratios.

4. Conclusion

The nanostructured RhNi catalysts, supported on a nanofibrous alumina, have proved to be highly active and stable catalysts for the DRM and DRM + H_2O reactions. Even when the catalysts were prepared by the impregnation method, the morphology of the support and the promotion by Rh allow the attainment of stable and disperse Ni particles. The addition of Rh to the formulation of Ni-based catalysts modifies the Ni-environment modifying the electronic properties, inhibiting the net formation of carbon, promoting the reducibility of Ni and avoiding the sintering of the metallic particles. Besides, the stability of the catalysts, in terms of time on stream, is considerably improved when Rh is incorporated. During the DRM + H_2O the overall carbon formation is drastically inhibited and adjustable H_2/CO ratios can be obtained.

Acknowledgements

MGD acknowledges the Spanish Minister of Education and Science for a FPI grant and for the financial support to the projects ENE2004-06176 and ENE2007-67926-C02-02/ALT. The authors are grateful to Dr. María Jesús Lázaro (ICB-CSIC, Zaragoza-Spain) for the TPR analysis.

References

[1] J.D. Holladay, J. Hu, D.L. King, Y. Wang., Catal. Today 139 (2009) 244–260.
[2] M. García-Diéguez, PhD thesis, University of Malaga, Spain, 2010.
[3] J.R. Rostrup-Nielsen, Catal. Today 18 (1993) 305–324.
[4] M.C.J. Bradford, M.A. Vannice, Catal. Rev. Sci. Eng. 41 (1999) 1–42.
[5] B. Pawelec, S. Damyanova, K. Arishtirova, J.L. Fierro, L. Petrov, Appl. Catal. A 323 (2007) 188–201.
[6] C.E. Daza, J.A. Jaime Gallego, F. Moreno, S. Mondragón, R. Moreno, Molina, Catal. Today 133–135 (2008) 357–366.
[7] K.Y. Koo, H.-S. Roh, Y.T. Seo, D.J. Seo, W.L. Yoon, S.B. Park, Appl. Catal. A 340 (2008) 183–190.
[8] E. Ruckenstein, Y.H. Hu, Appl. Catal. A 133 (1995) 149–161.
[9] G. Seo, M.H. Youn, I. Nam, S. Hwang, J.S. Chung, I.K. Song, Catal. Lett. 130 (2009) 410–416.
[10] S. Wang, G.Q. Lu, Energy Fuels 10 (1996) 896–904.
[11] N. Sahli, C. Petit, A.C. Roger, A. Kiennemann, S. Libs, M.M. Vetar, Catal. Today 113 (2006) 187–193.
[12] J. Zhang, H. Wang, A.K. Dalai, J. Catal. 249 (2007) 300–310.
[13] J.H. Bitter, K. Seshan, J.A. Lercher, J. Catal. 171 (1997) 279–286.
[14] M. García-Diéguez, I.S. Pieta, M.C. Herrera, M.A. Larrubia, L.J. Alemany, Appl. Catal. A 377 (2010) 191–199.

[15] M. García-Diéguez, I.S. Pieta, M.C. Herrera, M.A. Larrubia, L.J. Alemany, J. Catal. 270 (2010) 136–145.
[16] M. García-Diéguez, E. Finocchio, M.A. Larrubia, L.J. Alemany, G. Busca, J. Catal. 274 (2010) 11–20.
[17] J.R. Rostrup-Nielsen, Catal. Today 63 (2000) 159–164.
[18] Y.H. Hu, E. Ruckenstein, Adv. Catal. 48 (2004) 297–345.
[19] C.H. Bartholomew, Catal. Rev. Sci. Eng. 24 (1982) 67–112.
[20] J.R. Rostrup-Nielsen, Stud. Surf. Sci. Catal. 68 (1991) 85–101.
[21] K. Nagaoka, K. Seshan, K.-I. Aika, J.A. Lercher, J. Catal. 197 (2001) 34–42.
[22] M. García-Diéguez, I. Pieta, F. Sánchez-García, B. Guerrero-Klein, M.C. Herrera, M.A. Larrubia, L.J. Alemany, Proceedings XXI Simposio Iberoamericano de Catálisis (SICAT), Malaga, Spain, 2008, ISBN 978 84 691 4234 9, p. 1594.
[23] M. García-Diéguez, I.S. Pieta, M.C. Herrera, M.A. Larrubia, L.J. Alemany, Catal. Commun. 11 (2010) 1133–1136.
[24] Y.-G. Chen, K. Tomishige, K. Yokoyama, K. Fujimoto, Appl. Catal. A 165 (1997) 335–347.
[25] J.P. Contour, G. Mouvier, M. Hoogewys, C. Leclere, J. Catal. 48 (1977) 217–228.
[26] J.L.G. Fierro, J.M. Palacios, F. Tomas, Surf. Interface Anal. 13 (1988) 25–32.
[27] J.Z. Shyu, K. Otto, J. Catal. 115 (1989) 16–23.
[28] G. Li, L. Hu, J.M. Hill, Appl. Catal. A 301 (2006) 16–24.
[29] B. Scheffer, P. Molhoek, J.A. Moulijn, Appl. Catal. 46 (1989) 11–30.
[30] J.M. Rynkowski, T. Paryjczak, M. Lenik, Appl. Catal. A 106 (1993) 73–82.
[31] R. Molina, G. Poncelet, J. Catal. 173 (1998) 257–267.
[32] M. Ferrandon, A.J. Kropf, T. Krause, Appl. Catal. A 379 (2010) 121–128.
[33] D. Qin, J. Lapszcewiz, Catal. Today 21 (1994) 551–560.
[34] V.R. Choudhary, A.M. Rajput, Ind. Eng. Chem. Res. 35 (1996) 3934–3939.
[35] V.R. Choudhary, K.C. Mondal, Appl. Energy 83 (2006) 1024–1032.
[36] J. Wei, E. Iglesia, J. Phys. Chem. B 108 (2004) 4094–4103.